Formulation and rheological characterization of piezoelectric nanofluids

Mohamed Youssry [*], Sara Al-Abed, Raghad Abu Zannad, Maram M. Meslam, Rahaf Asad

Chemistry Program, Department of Chemistry and Earth Sciences, College of Arts and Sciences, Qatar University, Doha 2713, Qatar

ABSTRACT

We introduced a novel concept on energy harvesting nanofluids of hybrid piezoelectric ceramic and polymeric (BaTiO$_3$ and PVdF) materials in PDMS. Rheology, rheo-microscope and impedance spectroscopy complementary enabled the elucidation of the development of microstructure and probing the flow-induced structural transitions. Percolated CNTs enhanced the network mechanically and electrically and improved the output voltage (OV). Traces of PVdF further increased the OV to *ca.* 7.5 V in their hybrid suspensions.

1. Introduction

Piezoelectric materials are fascinating smart materials that reversibly convert the mechanical energy to electrical energy due to change in the molecular polarizability [1]. They are classified into different types including single crystal, ceramics, and polymeric materials and found applications in several domains including sensors, transducers, and electrical generators. Although the polymeric materials have much lower piezoelectric coefficient (d_{33}) than ceramic counterparts, the former are flexible, chemically, and mechanically stable, and can be easily processed into a large variety of configurations [2]. Among several examples, ceramic barium titanate (BaTiO$_3$) and polyvinyl difluoride (PVdF) are two interesting non-toxic piezoelectric materials with $d_{33} \approx 190$ and 37 pC N^{-1} [3,4]. They are promising in the energy harvesting applications when engineered in layered nanostructures to produce the so-called nanogenerators [5–10]. The current research focus on the solid-state structured films of piezoelectric materials that are deposited on a support to convert the mechanical stress into electrical energy [11]. In this study, we introduce a novel approach toward the formulation of piezoelectric hybrid flowable suspensions, highlighting the crucial tuning and systematic mixing of materials. The piezoelectric nanofluids are composed of hybrid ceramic BaTiO$_3$ and polymeric PVdF in addition to electrically conductive additives suspended in dielectric medium (polydimethylsiloxane; PDMS).

It is well stated that the carbon nanomaterials form a three-dimensional network of aggregates connected by links above a critical concentration; the so-called percolation threshold [12–16]. The aggregation mechanism and hence the network rigidity are sensitive to the particle size and morphology (aspect ratio), surface area and chemistry, and the compatibility between carbon particles and dispersing medium. In either open or dense network, the percolated dispersions can transmit the electrical current through the interlinks [17–20]. Hence, the carbon dispersions act as conductive matrix for transmitting the generated current due to poled piezoelectric materials [8,21]. Accordingly, it is crucial to precisely determine the percolation threshold and understand the aggregation mechanism of the selected multiwalled carbon nanotubes (CNTs) in PDMS under quiescent conditions. This type of dispersions commonly exhibits complex non-Newtonian flow behaviour that is linked with plausible structural transitions and the consequent variation of electrical conductivity under flow conditions [15,19,20,22,23].

Similarly, the ceramic BaTiO$_3$ particles aggregate in PDMS forming structured dispersions with higher d_{33} as the particles load increases on the expenses of tremendous increase in the network elasticity [11,24]. Moreover, prospective reorganization of aggregates may accompany the incorporation of BaTiO$_3$ particles onto the percolated network because of rupturing of weak CNTs interlinks [25]. Hence, the electrical conductivity of BaTiO$_3$/CNTs nanofluids should vary with the content of electrically insulating particles [26,27]. Tuning the relative composition is crucial in formulating a suspension with optimized properties. Guan et al. highlighted the improved dielectric properties of analogous ternary composites derived by optimizing the synergistic effects between the charge storage behaviour of BaTiO$_3$ and the charge transport behaviour of CNTs [28]. Such composite is prominent to act as

* Corresponding author.
E-mail address: myoussry@qu.edu.qa (M. Youssry).

piezoelectric nanofluid. Nevertheless, the anticipated fragility of BaTiO$_3$ network due to strong interaction between its particles and the dispersing medium (PDMS) [29] may lessen the piezoelectric efficiency of suspensions due to serious breaking up of network under flow conditions. To overcome this constraint, a flexible piezoelectric material such as PVdF [30] can be utilized as a binding additive to coherently the particle connectivity in sync with its inherent piezoelectric properties.

In this study, we aim to optimize the formulation and investigate the flow effect on the rheological and piezoelectric properties of hybrid suspensions composed of BaTiO$_3$, PVdF and CNTs in PDMS. The suspensions are systematically studied by rheology, rheo-impedance spectroscopy and rheo-microscopy to confer a complementary view for the precise selection of suspension composition and operational conditions.

2. Experimental section

2.1. Materials and preparation of suspensions

Barium titanate (BaTiO$_3$; BTO) has been synthesized and characterized as detailed in the Sections S.1 and S.2 in the Supplementary Material. Multiwalled carbon nanotubes (CNTs, >95%, outer diameter = 10–20 nm, length = 10–30 μm), polydimethylsiloxane (PDMS; viscosity = 48.0 mPa.s) and polyvinylidene difluoride (PVdF, >99.9%) were, respectively, purchased from US Research Nanomaterials, Inc, USA, SiSiB SILICONES, and TMAX Battery Equipment, China. All suspensions have been formulated using a planetary ball mill (Changsha Tianchuang Powder Technology Co., Ltd., China). In 15–mL agate jars with 10 agate balls (Ø 6 mm), weighted amounts of solid materials (CNTs, BaTiO$_3$, PVdF) were dispersed in PDMS by ball milling for 4 h at 500 rpm at ambient temperature.

2.2. Rheology and rheo-microscopy

The rheology of freshly prepared suspensions was examined by a rotational rheometer (Anton Paar MCR102, Austria) using stainless steel parallel-plate geometry (Ø 25 mm) at a gap size of 1 mm. The measurements were conducted at constant temperature (25 °C) controlled by Peltier system. After loading the suspensions on the geometry, a common protocol was followed to guarantee a consistency in the rheological measurements: (i) the suspensions were subjected to pre-shearing at 100 s^{-1} for 10 min, then left to relax for 10 min, in order to remove the shear history, (ii) the amplitude (strain) sweep test was done to determine the linear viscoelastic region (LVER), (iii) the frequency sweep test done at an amplitude value (γ_0) acquired from the amplitude sweep, and (iv) the flow curve, where the dependency of viscosity (η) on the shear rate ($\dot{\gamma}$) was recorded. The optical micrographs of suspensions, at rest and under shear flow, were collected by a homemade setup which is composed of inverted optical polarized microscope (Opto-Edu (Beijing) Co., Ltd, China) mounted underneath of two transparent glass plates (Ø 50 mm). The upper plate is rotating horizontally by the action of a gear motor and the bottom one moves vertically for gap adjustment and lies fixed during shear flow. The applied shear rate is calculated from the rotational speed (in rpm), gap size and the plate diameter, assuming that the gap is filled with the sample which is exposed to a homogenous laminar flow.

2.3. Rheo-electrical properties

Using a customized copper parallel plate geometry (Ø 25 mm), the impedance spectra of suspensions were simultaneously recorded by a potentiostat (Admiral Squidstat Plus, USA) at 50 mV. The output voltage of piezoelectric suspensions was measured using an open circuit potential mode. The two copper plates were electrically insulated and installed in the rheometer where the bottom stationary and upper rotating plats were connected to the potentiostat to record the impedance spectra and open circuit potential of suspensions, at rest and under

shear flow, as schematically depicted in Figure S3.
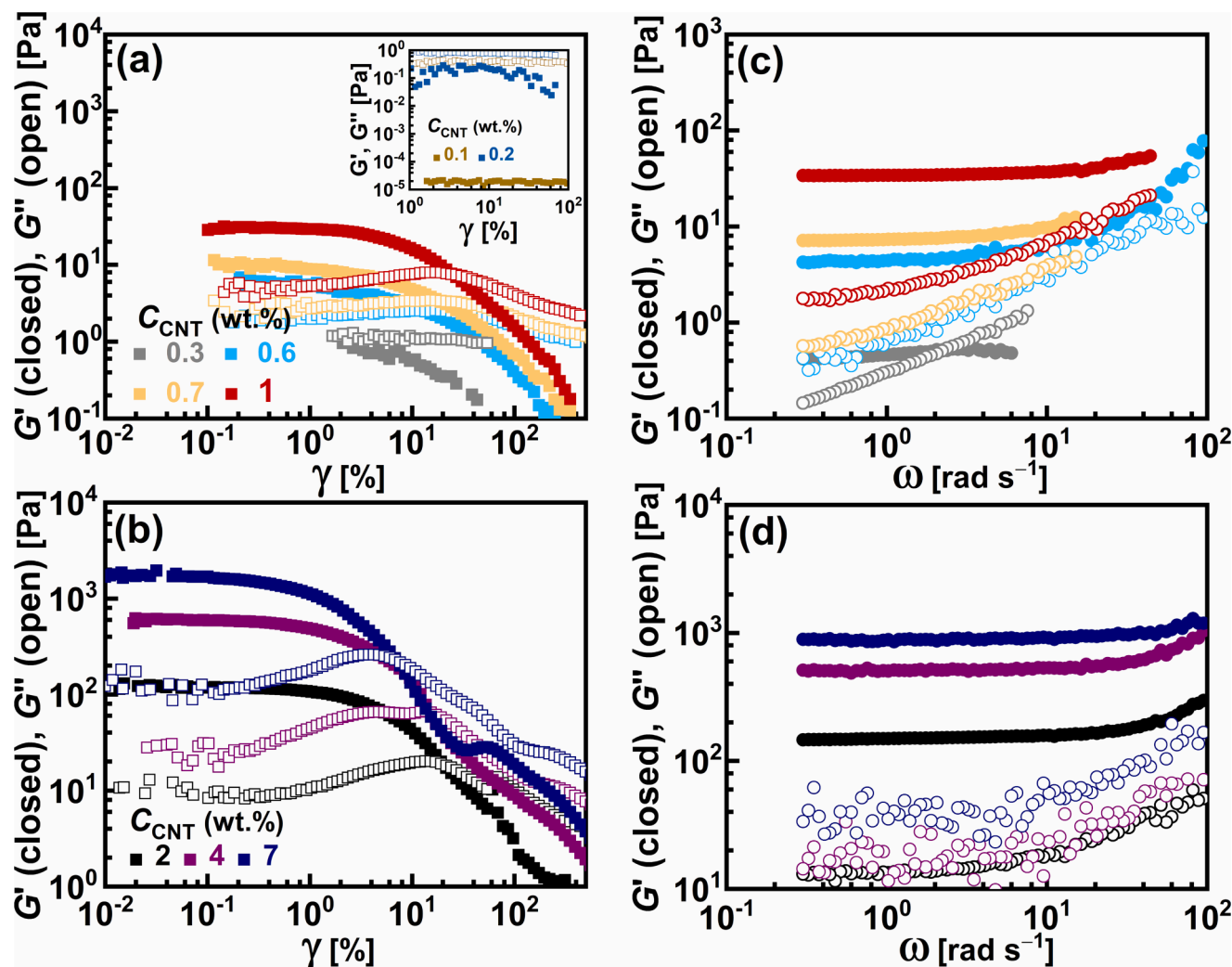
3. Results and discussions

In the current study, we systematically investigate the influence of each component (CNTs, BTO, PVdF) on the rheological, electrical, and piezoelectric properties of their suspensions in PDMS. Typically, PDMS is Newtonian fluid with zero-shear viscosity of about 48 mPa s over the temperature range of 10–100 °C (data not shown). We aim to formulate structured fluids with highest load of piezoelectric materials (viz., BTO and/or PVdF), in intrinsically dielectric medium (PDMS) possessing electrically conductive pathways (dispersions of CNTs). Therefore, we begin to investigate the properties of CNTs dispersions in PDMS to estimate the optimal CNTs content. The impact of BTO (and PVdF) content on the rheo-electrical properties of their suspensions is precisely examined.

3.1. Dispersions of carbon nanotubes in silicone oil

3.1.1. Aggregation mechanism

The development of microstructure in the dispersions of CNTs in PDMS is assessed by interpreting their dynamic rheology results at minimal perturbation. First, the dynamic strain sweep results for the dispersions over wide CNTs content (C_{CNT}) reveal a transition from pure liquid-like to viscoelastic gel-like behaviour above 0.3 wt% CNTs. This is evident from the independence of the elastic (G') and the viscous (G'') moduli on the applied strain (γ) at low C_{CNT} (inset of Fig. 1a), implying that the dispersions are not structured. The onset of structuring is likely to appear at 0.3 wt% CNTs when the dispersion displays a viscoelastic gel-like response signified by domination of G' over G'' and both moduli are independent of the applied deformation at low γ range (Fig. 1a). Beyond a critical strain (γ_c), the dynamic moduli decline before they crossover and eventually the dispersions behave typical liquid-like response featured by the domination of G'' over G' at higher γ range. This behaviour has been reported previously for analogous CNTs dispersions [31,32] and ascribed to strain-softening as a result of structural breaking up [20]. As can be seen from Fig. 1a, b, the magnitudes of the dynamic moduli rationally increase as the C_{CNT} rises, and the dispersions commonly exhibit transition from gel- to liquid-like response under large deformation. Though, the dispersions above 0.3 wt% CNTs exhibit strain-overshoot phenomenon [33] when G'' shows a maximum at intermediate γ before deviation from linear viscoelasticity. This phenomenon has been previously reported for aqueous dispersions of CNTs [31,32], and attributed to the formation of shear-induced transient network [34] that is weak enough to partially break up at slightly higher γ resulting in deviation of the dynamic moduli from linearity [35]. Obviously, the semidilute dispersions (Fig. 1a) exhibit trivial overshooting which becomes more pronounced for the concentrated dispersions (Fig. 1b). This trend is in agreement with the behaviour exhibited by aqueous dispersions of carbon blacks [23,36] and in contrast to the behaviour of nonaqueous dispersions of carbon nanofibers [20]. The particle-medium compatibility, floc size and the strength/extend of interaction between flocs are likely to be key factors in determining the extend of overshooting. The effectiveness of linear PDMS in dispersing CNTs, its low surface tension that permits enhanced wettability to the nanotubes [37] and the significant C-H-π interactions between methyl C-H bonds and the π-electron-rich surface of nanotubes [38] may be responsible for the structuring behavior of CNTs in PDMS.

Further insight into the development of equilibrium microstructure in CNTs dispersions is gained from the dynamic frequency sweep results at minimal perturbation (Fig. 1c,d). In tandem with the strain sweep data, the dilute dispersions (C_{CNT} < 0.3 wt%) show a typical liquid-like response as revealed from the domination of G'' over G' and dependency of dynamic moduli on the angular frequency (ω) (Fig. S4). At $C_{CNT} \approx 0.3$ wt%, the dispersion begins to exhibit a gel-like viscoelastic behaviour as evidenced by the domination of G' over G'' and both moduli are
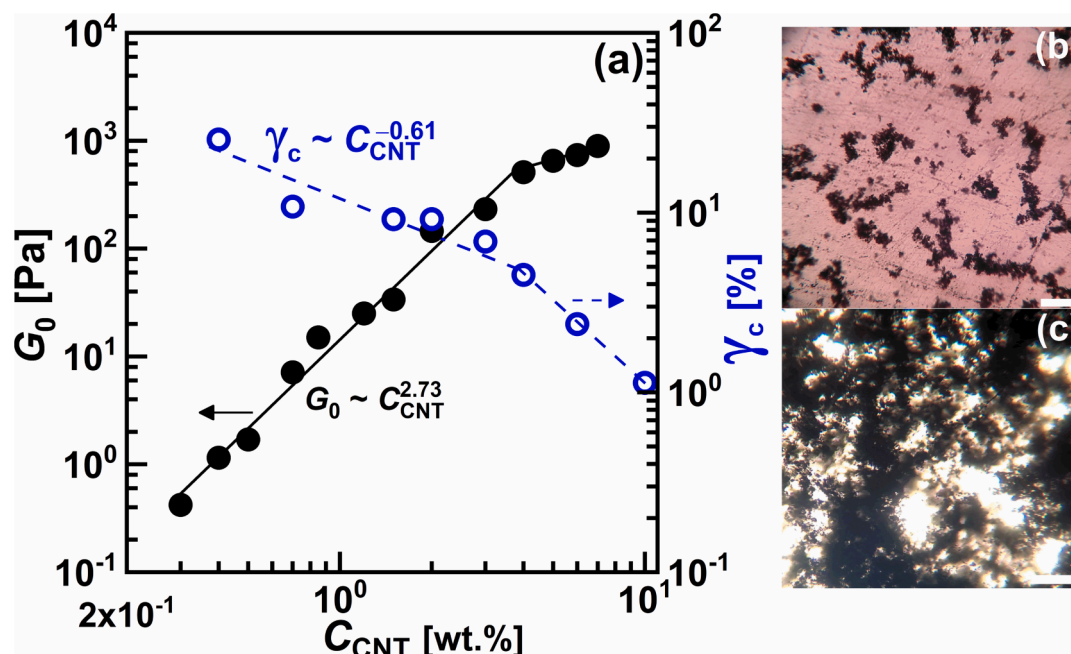
Fig. 1. The dynamic rheology of CNTs dispersions at 25 °C represented by (a,b) strain sweep tests at 1 Hz, and (c, d) frequency sweep tests at strain amplitudes (γ_0) in the linear viscoelastic regime for selected CNTs at of the elastic (G') and the viscous (G'') moduli on the angular frequency (ω) for selected dispersions over wide range of CNTs content (C_{CNT}) in weight per cent (wt.%).

constant over limited ω range before G'-G'' crossover at higher ω implying the transition to liquid-like fluid. The onset of gel-like behaviour at 0.3 wt% CNTs signifies the building up of a percolated network that is composed of connected bundles of aggregated nanotubes [32]. The high aspect ratio (*ca.* 1300 in average) of nanotubes and the wettability of PDMS are likely to induce the formation of anisometric interconnected wormlike bundles [37], as a building block of the three-dimensional percolated network. The semidilute dispersions (C_{CNT} = 0.3–1 wt%) unambiguously display a weak gel-like response characterizes by the significant dependency of G'' on ω over the entire range (Fig. 1c). As the CNTs content rises, this dependency weakens and G'' shows a minimum implying the transition to relatively stronger gel structure in the concentrated dispersions at C_{CNT} > 1 wt% (Fig. 1d). This viscoelastic behaviour resembles the one exhibited by highly concentrated dispersion of carbon blacks in silicone oil [35] and hard sphere colloidal suspensions [39]. At very short time (high ω), the hydrodynamic interaction is dominant by localized motion of individual bundles. The bundles are trapped in unbreakable cages of neighbouring ones in the percolated network, revealing the domination and independency of G' on the frequency at longer times (low ω). As the CNTs content rises, the number density of bundles increases so that the dynamics of trapped bundles dominate the frequency sweep when the bundles are more restricted in the cages [39]. Consequently, the concentrated dispersions turn stronger as evidenced by the weak dependency of G'' on the

frequency and disappearance of the G'–G'' crossover.

Fig. 2a depicts the dependence of the dynamic rheological parameters; namely the plateau modulus (G_0) and the critical strain (γ_c) on the CNTs content (C_{CNT}). The G_0 is extrapolated from the frequency sweep data at 0.3 rad s^{-1}, when the G' is considered to be independent of ω and the γ_c is obtained from the strain sweep results before the onset of overshooting [40]. Deeper insight on the development of the equilibrium microstructure in CNTs dispersions is gained from assessing the variation of G_0 and γ_c with C_{CNT}. The plateau modulus is linked with the network rigidity in terms of number density of links between bundles and the compactness of the network. The dilute dispersions (C_{CNT} < 0.3 wt%) lack the viscoelasticity and hence no G_0 can be disclosed due to the lack of connectivity between bundles (i.e., isolated bundles) as revealed from the optical micrograph of the non-percolated dispersion at 0.1 wt% CNTs (Fig. 2b). Above the percolating threshold, self-similar network of bundles linked by anisometric aggregated, rather than individual, nanotubes is formed. The optical micrograph of the percolated dispersion at 0.3 wt% CNTs supports this structural picture (Fig. 2c). As can be seen from Fig. 2a, the semidilute regime extends to 4 wt% CNTs when the G_0 varies with C_{CNT} revealing a scaling relationship: $G_0 \sim C_{CNT}^m$, with a positive exponent $m = 2.73$. Simulation study accounted for the nature of links between bundles based on the exponent of G_0 [41]. The network with links that resist the stretching but are free to rotate show an exponent of 2.1 ± 0.11, whilst that resist both stretching and rotating

Fig. 2. (a) variation of the plateau modulus (G_0) and the critical strain (γ_c) with the CNTs content (C_{CNT}), (b) and (c) the polarized optical micrographs of 0.1 and 0.3 wt% CNTs in PDMS, respectively. The lines are the best linear fit.

has an exponent of 3.75 ± 0.11. In the current CNTs/PDMS dispersion system, the exponent of 2.73 may be associated with semiflexible links that are bending during deformation (nonaffine deformation) [42]. This is consistent with the anticipated flexibility of nanotubes with high-aspect-ratio. Previous studies on aqueous dispersions of CNTs with aspect ratios = 80 [31] and 150 [32] showed comparable exponents of 2.6 and 2.3, respectively. Larger exponents (3.74, 4.3, 7.1) have been reported for suspensions of carbon nanotubes (aspect ratios = 45, 650, 200) in different dispersing media (epoxy, polyethylene oxide, poly-isobutylene), respectively [43–45]. Rahatekar et al. reported incomparable exponents of 2.4 and 6.5 for dispersions of long (aspect ratio = 1200) and short (aspect ratio = 80) CNTs in epoxy, respectively [46]. Accordingly, a correlation between the aspect ratio of nanotubes and the scaling exponent of G_0 of their dispersions cannot be drawn without taking into consideration the affinity of dispersing medium to the nanotubes, in contrast to the conclusion reported in previous study [14]. For instance, dispersions of spherical carbon blacks in silicone oil showed a scaling exponent of 2.6 [35], which is nearly identical to the one exhibited by the current dispersion system. In both types of networks, the interlinks are structured aggregates rather than individual units.

In the semidilute regime, γ_c similarly scales with C_{CNT} as: $\gamma_c \sim C_{CNT}^n$, with a negative exponent $n = -0.61$ (Fig. 2a), in agreement with the theoritical exponent (-0.50) predicted for interconnected network of bundles [32] and slightly higher than those reported for dispersions of long felxible carbon nanotubes (-0.30) [46] and nanofibers (-0.40) [20]. Although the interaction between bundles increases with the CNTs content, the critical strain declines, implying the fragility of the network. This evident by the strong drop in γ_c beyond 4 wt% CNTs when the dispersions enter the concetrated regime (Fig. 2a). The weak dependence of G_0 on the CNTs content above 4 wt% is in tandem with the trend of γ_c, implying the increased number density of bundles so that a staurated network is formed.

The percolated network of CNTs dispersions in the semidiluted regime can be viewed as fractals of interconnected bundles linked by aggregated nanotubes. According to Shih model [47], the positive and negative exponents of G_0 and γ_c, respectively, are consistent with strong-link regime in which the viscoelasticity of dispersions is dominant by

stronger interbundle links (viz. nanotubes) rather than intrabundle ones. The fractal dimension (D_f) of the bundles and the relative contributions of intrabundle and and interbundle links (β) have been related to the scaling exponents m and n thrrough Morbidelli model [48]:
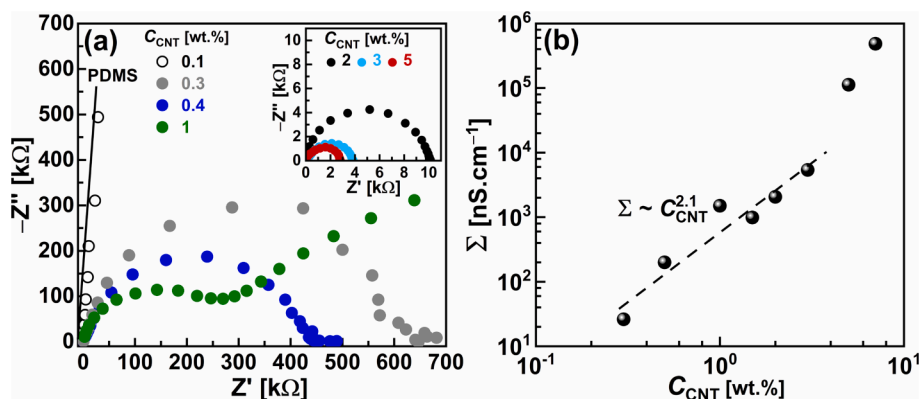
$$D_f = 3 - \frac{2}{m+n} \tag{1}$$

$$\beta = \frac{2m}{m+n} \tag{2}$$

Using Eq. (1), D_f is found to be 2.05, in a preferct agreement with the theoritical value predict for reaction-limited aggregation mechanism [49], in which a kinetically slow aggregation occurs through the interpenetration of aggregates resulting in denser aggregates. This structural picture is emphasized from the optical micrograph of a percolated dispersion as decpited in Fig. 2c. Similar D_f has been reported for dispersions of carbon nanotubes in epoxy [43] and and polyethylene oxide [44]. Based on Morbidelli, the parameter β falls in the range of 1 and 4.3, consistent with weak- and strong-link regimes, respectively [48]. The current dispersion system shows $\beta \approx 2.6$ (from Eq. (2), implying a comparable contribution of intrabundle and interbundle links in the elasticity of the dispersions in the semidilute regime. This supports the perception that links are composed of aggregated nanotubes, rather than free joined ones. Comparable values of the parameter β have been reported for protein gels in the transition between weak and strong regimes [50].

The dynamic rheology delineates the equilibrium microstructure of CNTs dispersions in PDMS at minimal perturbation. The dilute dispersions are composed of isolated anisometric aggregates of nanotubes (bundles). Above the percolation threshold, the number density of bundles increases and individual nanotubes (links) connect the bundles to form a three-dimensional network. This structural picture of CNTs dispersions in PDMS is further asserted by the variation of the impedance spectra and the extraploated electrical conductivity (Σ) of dispersions under the quscient conditions as depicted in Fig. 3. Notably, the non-percolated dispersions show linear Nyquist plot nearly similar to the behavior of dispersing medium (PDMS) as demonstrated for 0.1 wt% CNTs in Fig. 3a. The onset of structuring occurs at 0.3 wt% CNTs as obviously denoted from the perfect semicircle Nquist plot, in line with

Fig. 3. (a) Impedance spectra (represented by Nyquist plots) of CNTs dispersions at ambient temperature and 50 mV, and (b) dependency of the electrical conductivity (Σ) on the CNTs content (C_{CNT}). The values of Σ have been extraplotated by fitting the impedance spectra by an equivalent circuit as detailed in Section S.3 in the Supplementary Material.
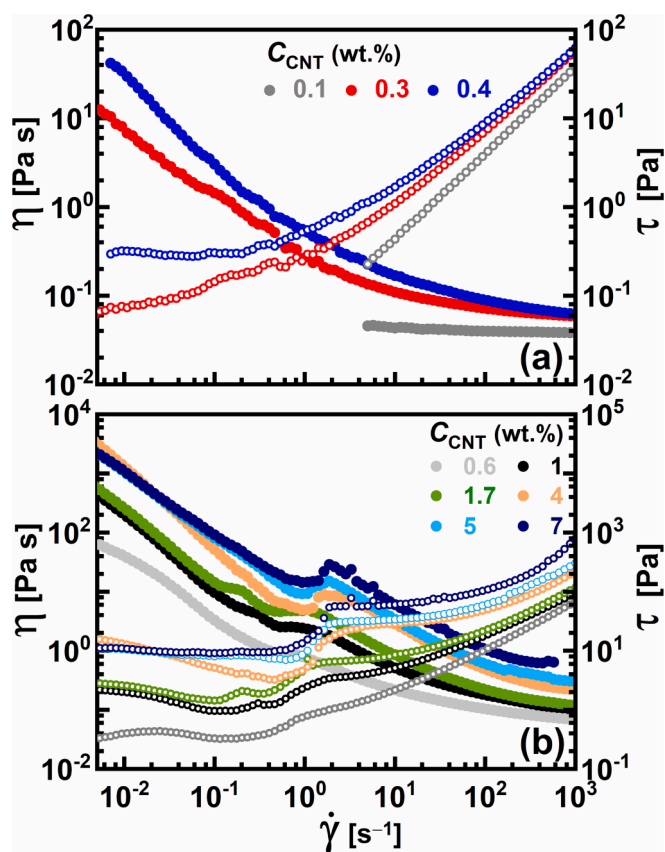
the rheology and rheo-microscopy data. This implies the onset of bulding up of electrical pathways (viz., percolated netwrok) rendering the dispersions electeically conductive. As the CNTs content rises, the semicircles turn narrower (inset of Fig. 3a) due to the progressive growth and increased number denisty of the connected aggregates with numerous pathways enhancing the transport of electrical current and hence rendering the dispersions much more conducive. Similar trend has been reported for analogous dipsersions of carbon blacks [19,23,36], nanofibers [20] and nanotubes [13,17].

Fig. 3b quantitatively demonstrates the dependency of the electric conductivity (Σ) of dispersions on the CNTs content. At $C_{CNT} < 0.3$ wt%, the dispersions do not show semicircle and hence no conductivity can be extrapolated. At $C_{CNT} \geq 0.3$ wt%, the electric conductivity linearly increases displaying a power-law relation: $\Sigma \sim C_{CNT}^l$, with an exponent $l = 2.1$. This exponent is in excellent agreement with the theoretical one ($l = 2$) reported for the percolated network [51] and experimental values ($l = 2.2$ and 2.3) exhibited by CNT nanocomposites [52,53] and carbon black suspensions [19].

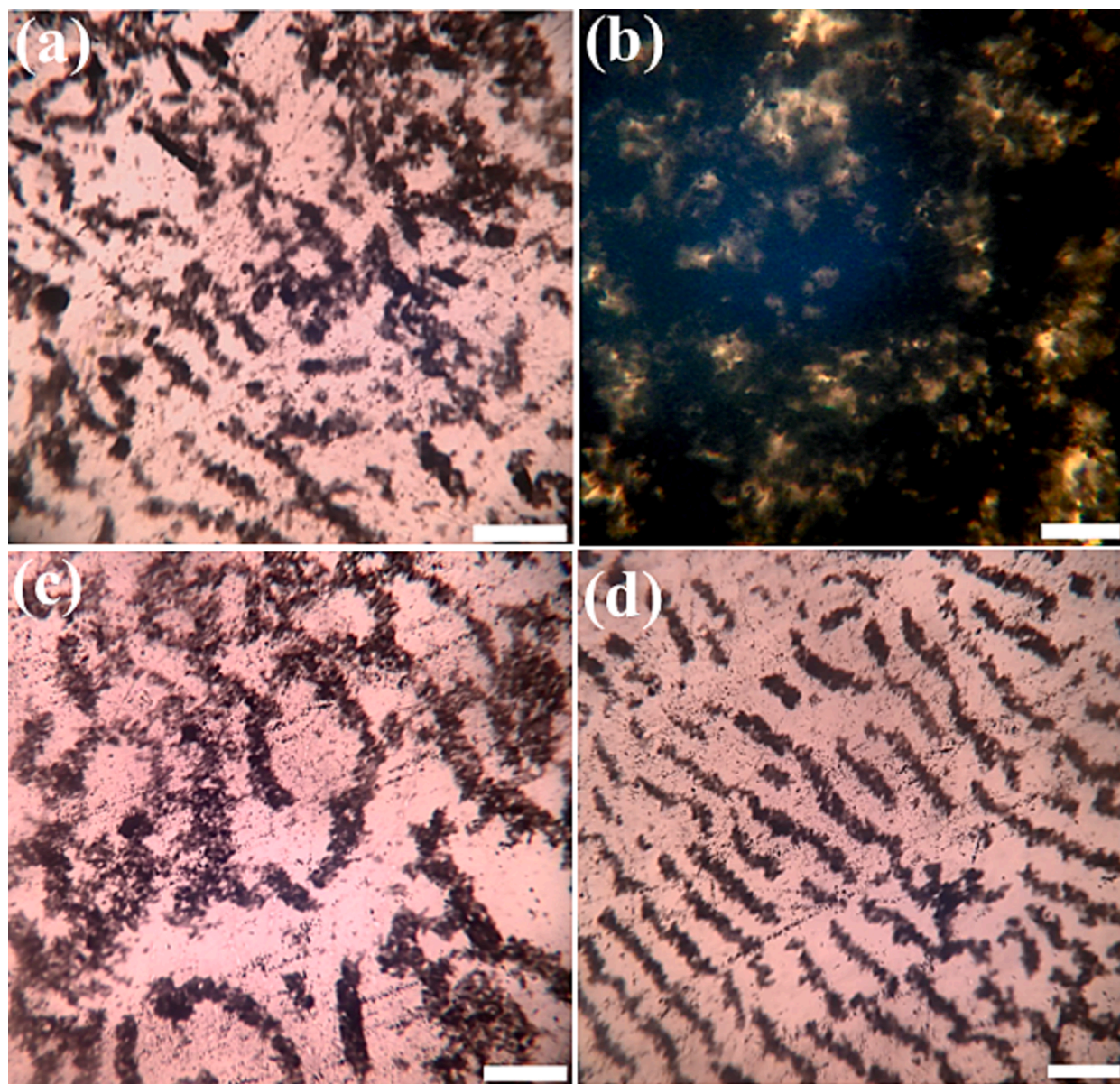### 3.1.2. Shear-induced structural transitions

The microstructure of CNT dispersions at equilibrium has been congruently investigated by dynamic rheology, rheo-microscopy and rheo-impedance spectroscopy. The dilute dispersions are composed of anisometric small aggregates that grow up and interconnect by nanotubes at 0.3 wt% CNTs forming 3D percolated network. The rheological and electrical properties of dispersions amend in the semidilute regime (0.3 wt% $\leq C_{CNT} < 4$ wt%) due to the increased number density of connected bundles before reaching the saturation at 4 wt% CNTs.

The steady rheology, in turn, brings to light the impact of continous shear flow on the microstructure and plausible shear-induced structural transition in the dispersions. Fig. 4 demonstrates the flow curves for selelcted CNTs dispersions, in terms of variation of steady shear viscoisty (η) and stress (τ) with the shear rate (γ̇). The dilute dispersion at 0.1 wt% CNTs obviously shows typical Newontian behaviour where η is constant over the entire range of γ̇ (Fig. 4a). This is linked with non-percolated network of isolated bundles. Once the dispersions turn percolated (0.3 and 0.4 wt%. CNTs), non-Newtonian (shear-thinning) behavior emerges over low and moderate shear rate range before turning into Newtonian one at higher shear rates (Fig. 4a). Such shear-thinning behavior is linked with the breaking up of the percolated netwrok into smaller anisometric bundles that are likely to align with the shear flow at higher shear rates. The rheo-optical micrograph of the dispersion at 0.3 wt% CNTs (Fig. 5a) argues such shear-induced structural breaking up in agreement with previous research on analogous colloidal dispersions [54,55]. The broken bundles are relatively small enough to display Newtonian response as obviously seen from the linear steep increase in the shear stress at higher shear rates (Fig. 4a).

Fig. 4. Variation of shear viscosity (η; solid circles) and stress (τ; open circles) with the applied shear rate (γ̇) for selected CNTs dispersions at 25 °C.

At $C_{CNT} \geq 0.6$ wt%, the dispersions commonly exhibit a complex flow curve featured by three regimes; two shear-thinning regimes separated by shear-thickening at intermediate shear rates as revealed from Fig. 4b. Flocculated suspensions of carbon blacks [19,22,23,36,56], nanotubes [15,57,58] and nanofibers [20] exhibited similar complex behavior which is associated with shear-induced structural transitions as described here. It should be noted that the network of the concentrated dispersions (e.g., 1 wt% CNTs) is more rigid than that of the diluted dispersions (e.g., 0.3 wt% CNTs) because of the densifing of the network by increasing the number density of connected larger bundles. This structural development is obvious when comparing the optical micrographs of the dilute 0.3 wt% (Fig. 2c) and concentrated 1 wt%

Fig. 5. Polarized optical micrographs of percolated CNTs dispersions at: (a) 0.3 wt% CNTs, $\dot{\gamma} = 10\ s^{-1}$, (b) 1 wt% CNTs, $\dot{\gamma} = 0\ s^{-1}$, (c) 1 wt% CNTs, $\dot{\gamma} = 1.2\ s^{-1}$, and (d) 1 wt% CNTs, $\dot{\gamma} = 14\ s^{-1}$ at ambient temperature. The scale bars correspond to 100 μm.

(Fig. 5b) CNTs dispersions at the quiescent conditions. Accordingly, the first thinning is mainly attributed to the breaking up of the percolated network into isolated anisometric bundles. This is evident from the micrograph of the percolated dispersion at 0.3 wt% CNTs which reveals the formation of relatively small anisometric aggregates that are likely aligned with the flow direction at higher shear rates. This dilute percolated dispersion does not show a shear-thickening behavior as the concentrated dispersions do. This is presumably ascribed to the relatively larger anisometric aggregates that result from the breaking up (first thinning) of the network of the concentrated dispersions. Fig. 5c supports this interpretation and reveals that the thickening is mainly due to the formation of eroded large anisomeric bundles in accordance with the response of analogous colloidal systems [20,23,56,59–61]. Beyond the thickening regime, the second thinning is mainly attributed to the alignment of the anisometric aggregates with the flow direction, as confirmed from the micrograph in Fig. 5e at higher shear rate. This behavior has been previously reported for analogous carbon suspensions [22,62,63], and ascribed to corresponding shear-induced structural transformations.

It should be noted that the dilute percolated dispersions do not show any hysteresis upon increasing (upscan) and decreasing (downscan) of the shear rate (Fig. S5), indicating the reversibility of shear-thinning due to the relatively small aggregates. The moderately concentrated dispersions (0.6–1.2 wt%. CNTs) exhibit perfectly reversible shear-thickening in contrast to the more concentrated ones ($C_{CNT} \geq 1.7$ wt %) which show progressive thixotropy and gradual diminishing of the thickening (in the downscan mode) as the CNTs content increases (Fig. S5). This behavior is in line with the structural picture aforementioned and mainly attribute to the increased local fluctuation of larger anisometric aggregates [64,65] or insufficient time for restructuring broken aggregates [22,56] in the concentrated dispersions.

The simultaneous measurement of the dispersions' electrical properties (represented by impedance spectra) under shear flow confers deep insight onto the plausible shear-induced microstructural transitions [19,20,23,36,66]. Fig. 6 depicts the variation of impedance spectra (represented by Nyquist plots) of the percolated dispersion at 1 wt% CNTs over wide range of shear rate. Notably, the semicircles gradually widen as the shear rate rises from 0.05 to 1 s^{-1}. At 2 s^{-1}, the width of the
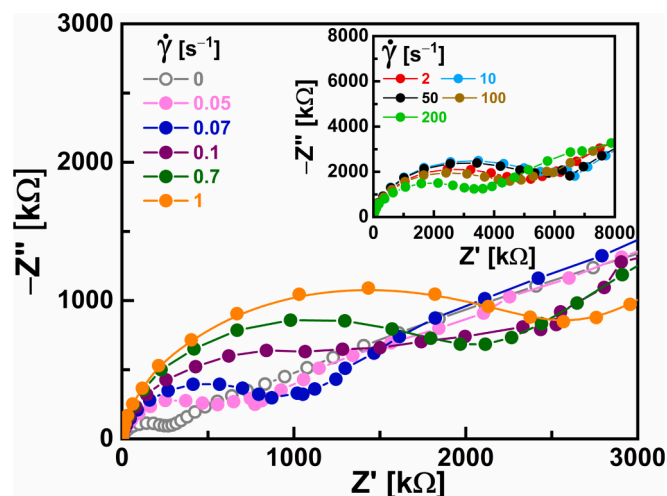
Fig. 6. Impedance spectra of the 1 wt% CNTs dispersion under flow at 25 °C and 50 mV.

semicircle abruptly enlarges and continues to increase up to 10 s⁻¹, before it mildly diminishes at higher shear rates (50–200 s⁻¹) as shown in the inset of Fig. 6. This behavior implies that the electrical conductivity of the dispersion gradually decreases with the shear rate, in line with the first shear-thinning, as a consequence of the breaking up of the percolated network into discrete bundles with ruptured electrical pathways. The sudden widening of semicircle at 2 s⁻¹, which lies at the end of thickening regime (see Fig. 4b), indicates a drop in electrical conductivity which may ascribe to complete rupturing of the pathways. The trivial recovery of electrical conductivity beyond 10 s⁻¹, in line with the second thinning regime, may be due to the existence of some randomly distributed bundles [13] rather than proper pathways of nanotubes as confirmed from Fig. 5d.

To recap, the CNTs/PDMS dispersions are mechanically and electrically percolated at 0.3 wt% CNTs. The percolated dispersions are essentially composed of bundles of aggregated nanotubes

interconnected by links of aggregated nanotubes under the quiescent conditions. Under flow, the network is broken up into isolated anisometric bundles exhibiting shear-thinning and lowered conductivity. Moderate shearing simulates a thickening behaviour when the number density of bundles is high enough to interact whilst the electrical conductivity is lower due to absence of real electrical pathways. Further shearing induces second thinning when the anisometric bundles align, while some randomly distributed ones fulfil some degree of connectivity enough to somewhat rectify the electrical conductivity.

3.2. Piezoelectric suspensions

It is believed that the optimal piezoelectric suspension is the one that contains the highest load of piezoelectric material (BTO and/or PVdF) that is homogenously distributed in the conductive percolated matrix, and yet flowable. Accordingly, we investigate the impact of systematic addition of piezoelectric material to a percolated dispersion on the rheological and the rheo-impedance properties of suspensions.

First, it is worth to investigate the rheological behaviour of BTO dispersions in PDMS in order to estimate the influence of BTO content (C_{BTO}) on the network rigidity. As can be seen from Fig. S6a, the BTO dispersions are liquid-like up to 10 wt%. At $C_{BTO} \geq 20$ wt%, the dispersions are gel-like (Fig. 7a) as evident from the independency of the dynamic moduli on the applied strain over low strain range. The BTO dispersions turn flowable above a critical strain when the dynamic moduli start to decrease after a crossover. This sol-gel transition is confirmed from the frequency sweep data in the LVER as depicted in Fig. 7b. The dispersions are not structured below 20 wt% BTO when G'' is higher than G' and both moduli are dependent on ω (Fig. S6b). The onset of structuring occurs at 20 wt% BTO when G' is higher than G'' over low ω range before G'-G'' crossover appears at moderate ω. This is a feature for weak gel-like dispersion which turns stronger as the BTO content increases as evident from the domination of G' over G'' and the independency of the dynamic moduli of ω (Fig. 7b). The plateau modulus (G_0) exhibits a strong monotonic increase from 20 to 40 wt% BTO before it nearly shows some independency on the BTO content beyond 40 wt% as depicted in Fig. 7c. In line with the dynamic rheology, the steady rheology reveals that the 20 wt% BTO is a critical concentration at
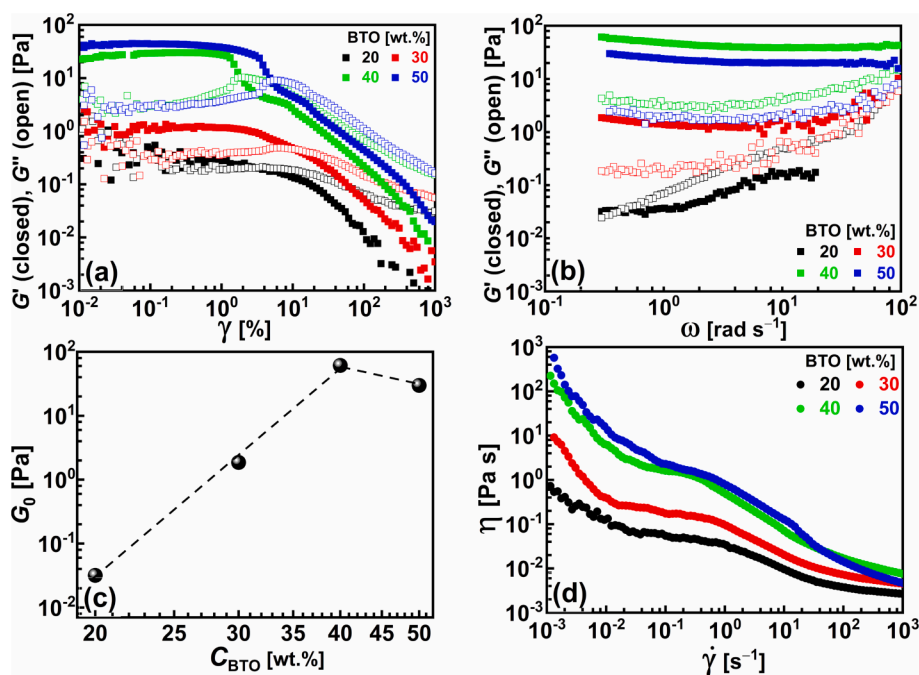

Fig. 7. (a) strain sweep, (b) frequency sweep, (c) variation of the plateau modulus (G_0) with the BTO content (C_{BTO}), and (d) flow curve of BTO dispersions in PDMS at 25 °C.

which the flow behaviour of the dispersions transforms from Newtonian (Fig. S6c) to non-Newtonian (Fig. 7d) behaviour implying the transition from non-structured (discrete aggregates) to structured (network of aggregates) dispersions. The structured dispersions (at $C_{BTO} \geq 20$ wt%) show complex non-Newtonian flow curves featured by two shear-thinning regimes separated by thickening regime over wide range of intermediate shear rate. Similar behaviour has been shown by BTO dispersions in ammonium polyacrylate [67], and the authors ascribed the first thinning behaviour to breaking up of aggregates. The BTO network is likely to be fragile enough to be broken at relatively low shear rates before entering the thickening regime which may originate from interacting broken aggregates. The extent of thickening regime may be linked with the number density of broken aggregates. Therefore, the relatively dilute dispersion (e.g., 20 wt% BTO) shows wider thickening regime than that exhibited by concentrated dispersion (e.g., 50 wt% BTO). The broken aggregates may align as the shear rate further increases, showing a second thinning regime.
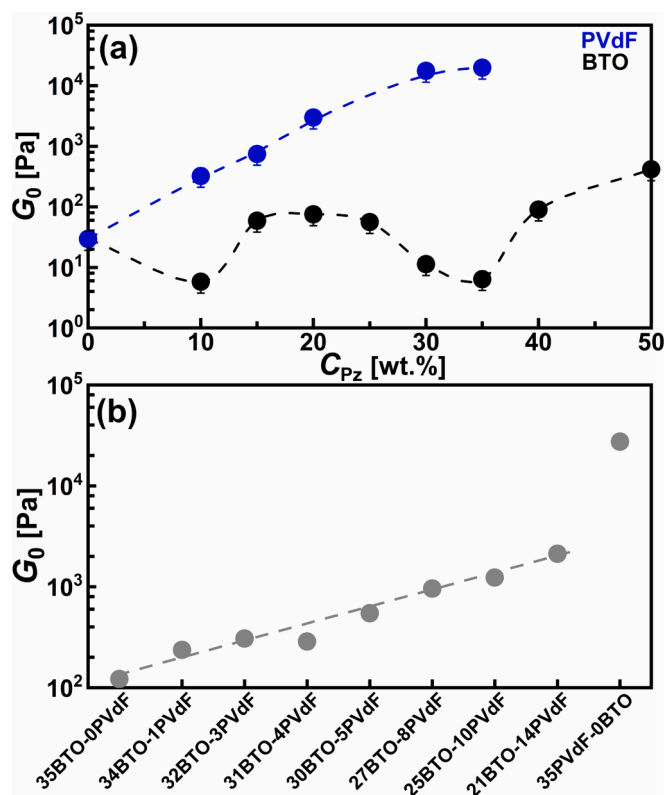
To optimize the formulation of piezoelectric nanofluids, a systematic addition of piezoelectric materials (BTO, PVdF and their mixture) to a percolated CNTs dispersion has been followed. The impact of addition of piezoelectric materials on the network elasticity (expressed by G_0) of their suspensions with 1 wt% CNTs (well above the percolating threshold) is depicted in Fig. 8. The elasticity of BTO-based suspensions irregularly varies with BTO content (Fig. 8a). A small (10 wt%) addition of BTO results in *ca.* 75% drop in the elasticity of the formulated suspension in comparison to the pure CNTs dispersion. This drop may ascribe to the penetration of small BTO aggregates onto the percolated carbon network [21], leading to link rupturing. When the amount of BTO is increased, G_0 is recovered and remains stable over the concentration range of 15–25 wt% BTO. The larger BTO aggregates (or

network) are likely to synergistically reinforce the CNTs network, resulting in suspensions with comparable elasticity to that of pure CNTs dispersion. At $C_{BTO} > 25$ wt%, G_0 declines again exhibiting a minimum at 35 wt% before it increases at higher BTO concentration (Fig. 8a). The 25 wt% BTO seems to be the saturation content above which the CNTs network cannot sustain the growth of BTO network, and the synergism diminishes. At $C_{BTO} > 35$ wt%, the CNTs and BTO aggregates cooperatively reinforce the network of their suspensions and rigid hybrid network forms. It is worth noting that the suspensions at 10 and 35 wt% BTO have nearly the lowest values of G_0, suggesting the utilization of 35 wt% BTO in the formulation of piezoelectric nanofluids, in accordance with previous study [8].

The PVdF-based suspensions are much more elastic than their BTO-based counterparts as revealed from the monotonic increase of G_0 with the PVdF content as shown in Fig. 8a. In comparison, G_0 of PVdF-based suspensions are two to four decades higher at the same load of piezoelectric material. This behaviour may ascribe to the unique compatibility between PVdF and PDMS which induces the formation of structured polymer matrix in which the percolated nanotubes are distributed [52,68].
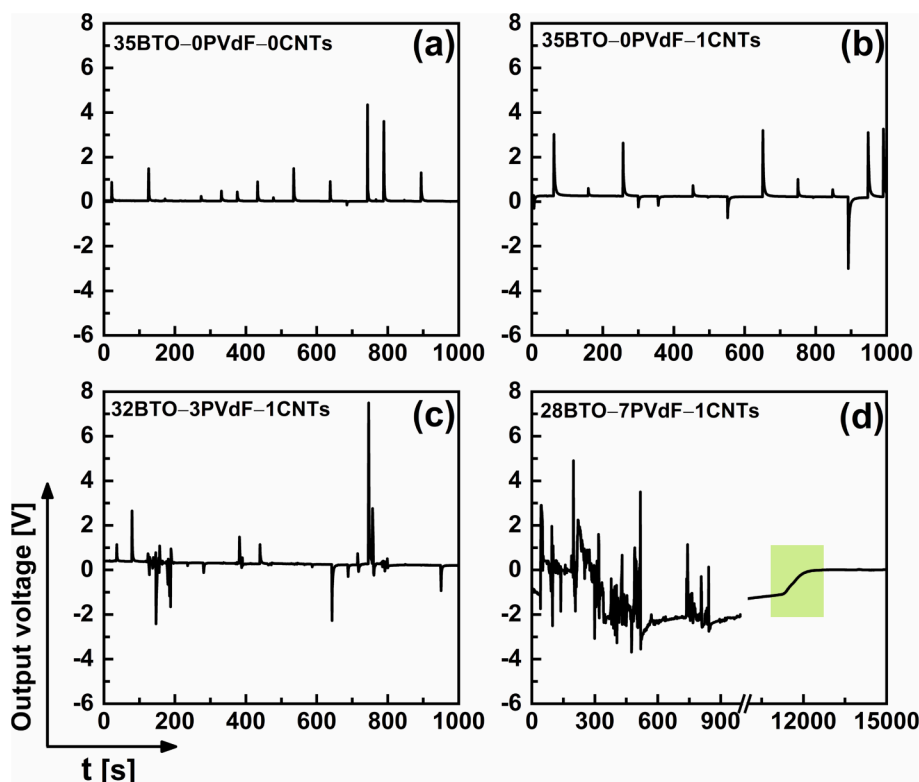
It is well stated that the ceramic BaTiO$_3$ is more efficient piezoelectric material than the polymeric PVdF as indicated from their intrinsic piezoelectric constants; $d_{33} = 190$ and 24–37 pC N^{-1}, respectively [3,4]. Indeed, the network rigidity of BaTiO$_3$-based suspensions is much less than their PVdF-based analogous; however, the steady rheology of these suspensions under continuous flow conditions may reveal peculiar shear-induced structural changes that require to be deliberately probed. Qualitatively, both of BTO and PVdF-based suspensions commonly show a three-regime flow curve: two thinning regimes separated by thickening one, as depicted in Fig. S7a, b. Considering the 1 wt% CNTs as a reference, the thickening regime of BTO-based suspensions shifts to lower shear rates (Fig. S7a), whilst shifts to higher rates in the PVdF-based ones (Fig. S7b). According to these differences, it is worth to examine the rheological properties of hybrid suspensions that are composed of both piezoelectric materials at fixed solid content (35 wt% as revealed from the dynamic rheology) and conductive additive (1 wt%. CNTs). Fig. 8b demonstrates the impact of replacing amounts of BTO by equivalents of PVdF on the trend of G_0 for selected hybrid suspensions. Obviously, the network rigidity of the hybrid suspensions rises as the amount of replaced PVdF increases due to the reinforcement of the network by the polymer chains that may cooperatively interact with the CNTs network. The role of added PVdF is evident from the flow curve of hybrid suspensions as depicted in Fig. 6Sc. The thickening regime diminishes and shifts to higher shear rates as the content of polymer additive increases. The impact of PVdF on the electrical properties of the hybrid suspensions under quiescent conditions and under flow is crucial in elucidating the equilibrium microstructure and plausible shear-induced structural transitions.

Preliminary investigation on the piezoelectric properties of some selected hybrid suspensions is displayed in Fig. 9 in terms of the variation of the output voltage (OV) with time. Assuming the amounts of samples are constant, the open circuit (OC) tests have been conducted in the rheometer geometry that is connected to the potentiostat as described in the Experimental Section. In this study, we investigate the impact of deformation due to sample loading and the relaxation of output voltage with time. Fig. 9a demonstrates the OV of CNTs-free dispersion of BTO at 35 wt% in PDMS. The BTO dispersion produces a positive voltage of *ca.* 4.4 V in accordance with previous report [10]. Upon adding CNTs, the suspension exhibits positive and negative OV range from 3.2 to −3.0 V as shown in Fig. 9b. Luo et al. reported similar trend for analogous suspensions and highlighted the impact of a critical content of conductive additive (carbon black) at which the piezoelectric properties are maximized [8]. In our suspension, the slight decrease in the OV upon adding CNTs may be linked to a ruptured BTO network due to large CNTs aggregates. Interestingly, the hybrid BTO-PVdF suspension generates higher OV of *ca.* 7.5 V (Fig. 9c), which is nearly double

Fig. 8. Effect of the content of piezoelectric materials (C_{Pz}) on the plateau modulus (G_0) of their suspensions with 1 wt% CNTs in PDMS at 25 °C: (a) pure BTO and PVdF, and (b) hybrid piezoelectric suspensions. The composition of hybrid suspensions is recognized from its name: for instance, 34BTO-1PVdF denotes 34 wt% BTO and 1 wt% PVdF, etc. The dashed lines are a guide for eyes.

Fig. 9. The output voltage generated from various piezoelectric suspensions in PDMS at ambient temperature, after loading the samples in the geometry to equilibrate over time duration (t). The composition of suspensions is recognized from its name: for instance, 35BTO-0PVdF-0CNTs denotes 35 wt% BaTiO$_3$ without PVdF and CNTs, etc.

the voltage produced from the PVdF-free suspension. This implies that the hybrid piezoelectric materials (BTO and PVdF) reinforce each other to produce a maximized piezoelectric activity [69].

The suspensions obviously generate unstable output voltage. This instability may attribute to a random rotational polarization [70] of the piezoelectric active materials (BTO and/or PVdF) when the suspensions are either under unsteady deformation or relaxation. Fig. 9d shows a complete relaxation test for an example of a hybrid suspension over few hours. The suspension completely relaxes and the shear-induced voltage drops gradually to zero after about 3.3 h in contrast to all conventional piezoelectric composites which generate a voltage only upon steady permanent deformation [4,7,71].

4. Conclusion

In this contribution, we attempt to introduce a systematic investigation for the formulation and properties of piezoelectric nanofluids made up of barium titanate (BaTiO$_3$; BTO), polyvinylidene difluoride (PVdF) with conductive multiwalled carbon nanotubes (CNTs) suspended in polydimethylsiloxane (PDMS). The CNTs/PDMS dispersion system is rheologically and electrically percolated at 0.3 wt% CNTs, at which 3D network of bundles are linked with anisometric aggregated nanotubes, which exhibits shear-induced structural transitions linked with variation of electrical conductivity under continuous flow. The BTO/PDMS system is structured at BTO content ($C_{BTO} \geq 20$ wt%), with much fragile network than analogous PVdF-based dispersions due to particle nature and compatibility with PDMS. Preliminary data on piezoelectric nanofluids emphasis the role of CNTs additive and the potency of hybrid mixture of BTO and traces of PVdF that produces an output voltage (OV) of *ca.* 7.5 V. This produced OV interestingly results from uncontrolled deformation due to sample loading, and decays to zero after 3.3 h. The structure and properties of piezoelectric nanofluids under controlled flow conditions are under investigation and will be the

aim of future contribution.

CRediT authorship contribution statement

Mohamed Youssry: Conceptualization, Methodology, Supervision, Project administration, Funding acquisition, Writing – original draft, Writing – review & editing. **Sara Al-Abed:** Data curation, Investigation, Visualization. **Raghad Abu Zannad:** Data curation, Resources, Investigation. **Maram M. Meslam:** Data curation, Resources, Investigation. **Rahaf Asad:** Data curation.

Declaration of Competing Interest

The authors declare that they have no known competing financial interests or personal relationships that could have appeared to influence the work reported in this paper.

Data availability

No data was used for the research described in the article.

Appendix A. Supplementary data

Supplementary data to this article can be found online at https://doi.org/10.1016/j.molliq.2023.123186.

References

[1] K. Uchino, in: Advanced Piezoelectric Materials, Woodhead Publishing, 2010, pp. 1–85.

[2] V.F. Cardoso, C.M. Costa, D.M. Correia, E.O. Carvalho, N. Peřinka, P.M. Martins, R.M. Meira, T. Marques-Almeida, T. Rodrigues-Marinho, S. Lanceros-Mendez, in: K. Asadi (Ed.) Organic Ferroelectric Materials and Applications, Woodhead Publishing, 2022, p. 375-439.

[3] H. Jaffe, J. Am. Ceram. Soc. 41 (1958) 494, https://doi.org/10.1111/j.1151-2916.1958.tb12903.x.

[4] C. Wan, C.R. Bowen, J. Mater. Chem. A 5 (2017) 3091, https://doi.org/10.1039/C6TA09590A.

[5] H. Nagata, M. Yoshida, Y. Makiuchi, T. Takenaka, Jpn. J. Appl. Phys. 42 (2003) 7401, https://doi.org/10.1143/JJAP.42.7401.

[6] K.-I. Park, M. Lee, Y. Liu, S. Moon, G.-T. Hwang, G. Zhu, J.E. Kim, S.O. Kim, D.K. Kim, Z.L. Wang, K.J. Lee, Adv. Mater. 24 (2012) 2999, https://doi.org/10.1002/adma.201200105.

[7] K.N. Kim, J. Chun, S.A. Chae, C.W. Ahn, I.W. Kim, S.-W. Kim, Z.L. Wang, J.M. Baik, Nano Energy 14 (2015) 87, https://doi.org/10.1016/j.nanoen.2015.01.004.

[8] C. Luo, S. Hu, M. Xia, P. Li, J. Hu, G. Li, H. Jiang, W. Zhang, Energy Technol. 6 (2018) 922, https://doi.org/10.1002/ente.201700756.

[9] K.K. Sappati, S. Bhadra, IEEE International Flexible Electronics Technology Conference (IFETC) 2019 (2019) 1–3, https://doi.org/10.1109/IFETC46817.2019.9073766.

[10] J. Zhou, X. Gou, D. Fan, J. Wang, Z. Wan, ACS Appl. Mater. Interfaces 14 (2022) 38105, https://doi.org/10.1021/acsami.2c04196.

[11] N. Sezer, M. Koç, Nano Energy 80 (2021), 105567, https://doi.org/10.1016/j.nanoen.2020.105567.

[12] T. Amari, K. Watanabe, J. Rheol. 34 (1990) 207, https://doi.org/10.1122/1.550124.

[13] M.D. Lima, M.J. Andrade, V. Skákalová, C.P. Bergmann, S. Roth, J. Mater. Chem. 17 (2007) 4846, https://doi.org/10.1039/B710417K.

[14] D. Wu, L. Wu, W. Zhou, Y. Sun, M. Zhang, J. Polym. Sci., Part B: Polym. Phys. 48 (2010) 479, https://doi.org/10.1002/polb.21909.

[15] S. Majumdar, R. Krishnaswamy, A.K. Sood, PNAS 108 (2011) 8996, https://doi.org/10.1073/pnas.1018685108.

[16] J.J. Richards, J.B. Hipp, J.K. Riley, N.J. Wagner, P.D. Butler, Langmuir 33 (2017) 12260, https://doi.org/10.1021/acs.langmuir.7b02538.

[17] C. Penu, G.H. Hu, A. Fernandez, P. Marchal, L. Choplin, Polym. Eng. Sci. 52 (2012) 2173, https://doi.org/10.1002/pen.23162.

[18] B. Akuzum, P. Singh, D.A. Eichfeld, L. Agartan, S. Uzun, Y. Gogotsi, E.C. Kumbur, ACS Appl. Mater. Interfaces 12 (2020) 5866, https://doi.org/10.1021/acsami.9b19739.

[19] M. Youssry, L. Madec, P. Soudan, M. Cerbelaud, D. Guyomard, B. Lestriez, Phys. Chem. Chem. Phys. 15 (2013) 14476, https://doi.org/10.1039/C3CP51371H.

[20] M. Youssry, D. Guyomard, B. Lestriez, Phys. Chem. Chem. Phys. 17 (2015) 32316, https://doi.org/10.1039/C5CP06303E.

[21] B.-S. Lee, J. Yoon, C. Jung, D.Y. Kim, S.-Y. Jeon, K.-H. Kim, J.-H. Park, H. Park, K.H. Lee, Y.-S. Kang, J.-H. Park, H. Jung, W.-R. Yu, S.-G. Doo, ACS Nano 10 (2016) 2617, https://doi.org/10.1021/acsnano.5b07674.

[22] A.S. Negi, C.O. Osuji, Rheol. Acta 48 (2009) 871, https://doi.org/10.1007/s00397-008-0341-9.

[23] M. Youssry, F.Z. Kamand, M.I. Magzoub, M.S. Nasser, RSC Adv. 8 (2018) 32119, https://doi.org/10.1039/C8RA05446K.

[24] J.E.Q. Quinsaat, T. de Wild, F.A. Nüesch, D. Damjanovic, R. Krämer, G. Schürch, D. Häfliger, F. Clemens, T. Sebastian, M. Dascalu, D.M. Opris, Composites, Part B 198 (2020), 108211, https://doi.org/10.1016/j.compositesb.2020.108211.

[25] M. Youssry, L. Madec, P. Soudan, M. Cerbelaud, D. Guyomard, B. Lestriez, J. Power Sources 274 (2015) 424, https://doi.org/10.1016/j.jpowsour.2014.10.076.

[26] E. Ricohermoso, F. Rosenburg, F. Klug, N. Nicoloso, H.F. Schlaak, R. Riedel, E. Ionescu, Open Ceram. 5 (2021), 100057, https://doi.org/10.1016/j.oceram.2021.100057.

[27] O. Malek, J. González-Julián, J. Vleugels, W. Vanderauwera, B. Lauwers, M. Belmonte, Mater. Today 14 (2011) 496, https://doi.org/10.1016/S1369-7021(11)70214-0.

[28] S. Guan, H. Li, S. Zhao, L. Guo, Compos. Sci. Technol. 158 (2018) 79, https://doi.org/10.1016/j.compscitech.2017.12.038.

[29] D. Meisak, M. Kinka, A. Plyushch, J. Macutkevič, A. Zarkov, S. Schaefer, A. Selskis, V. Samulionis, P. Kuzhir, J.r. Banys, V. Fierro, A. Celzard, ACS Omega 8 (2023) 13911, https://doi.org/10.1021/acsomega.3c00321.

[30] L. Lu, W. Ding, J. Liu, B. Yang, Nano Energy 78 (2020), 105251, https://doi.org/10.1016/j.nanoen.2020.105251.

[31] I.A. Kinloch, S.A. Roberts, A.H. Windle, Polymer 43 (2002) 7483, https://doi.org/10.1016/S0032-3861(02)00664-X.

[32] L.A. Hough, M.F. Islam, P.A. Janmey, A.G. Yodh, Phys. Rev. Lett. 93 (2004), 168102, https://doi.org/10.1103/PhysRevLett.93.168102.

[33] K. Hyun, S.H. Kim, K.H. Ahn, S.J. Lee, J. Non-Newtonian Fluid Mech. 107 (2002) 51, https://doi.org/10.1016/S0377-0257(02)00141-6.

[34] M. Youssry, L. Coppola, I. Nicotera, C. Morán, J. Colloid Interface Sci. 321 (2008) 459, https://doi.org/10.1016/j.jcis.2008.02.023.

[35] M. Kawaguchi, M. Okuno, T. Kato, Langmuir 17 (2001) 6041, https://doi.org/10.1021/la010560r.

[36] M. Meslam, A.A. Elzatahry, M. Youssry, Colloids Surf., A (2022) 129376, https://doi.org/10.1016/j.colsurfa.2022.129376.

[37] D.H. Flagg, T.J. McCarthy, Langmuir 35 (2019) 13396, https://doi.org/10.1021/acs.langmuir.9b02467.

[38] A. Beigbeder, M. Linares, M. Devalckenaere, P. Degée, M. Claes, D. Beljonne, R. Lazzaroni, P. Dubois, Adv. Mater. 20 (2008) 1003, https://doi.org/10.1002/adma.200701497.

[39] T.G. Mason, D.A. Weitz, Phys. Rev. Lett. 75 (1995) 2770, https://doi.org/10.1103/PhysRevLett.75.2770.

[40] F. Bossler, J. Maurath, K. Dyhr, N. Willenbacher, E. Koos, J. Rheol. 62 (2018) 183, https://doi.org/10.1122/1.4997889.

[41] M. Sahimi, S. Arbabi, Phys. Rev. B 47 (1993) 703, https://doi.org/10.1103/PhysRevB.47.703.

[42] D.A. Head, F.C. MacKintosh, A.J. Levine, Phys. Rev. E 68 (2003), 025101, https://doi.org/10.1103/PhysRevE.68.025101.

[43] F. Khalkhal, P.J. Carreau, Rheol. Acta 50 (2011) 717, https://doi.org/10.1007/s00397-010-0527-9.

[44] T. Chatterjee, R. Krishnamoorti, Phys. Rev. E 75 (2007), 050403, https://doi.org/10.1103/PhysRevE.75.050403.

[45] E.K. Hobbie, D.J. Fry, Phys. Rev. Lett. 97 (2006), 036101, https://doi.org/10.1103/PhysRevLett.97.036101.

[46] S.S. Rahatekar, K.K. Koziol, S.R. Kline, E.K. Hobbie, J.W. Gilman, A.H. Windle, Adv. Mater. 21 (2009) 874, https://doi.org/10.1002/adma.200802670.

[47] W.-H. Shih, W.Y. Shih, S.-I. Kim, J. Liu, I.A. Aksay, Phys. Rev. A 42 (1990) 4772, https://doi.org/10.1103/PhysRevA.42.4772.

[48] H. Wu, M. Morbidelli, Langmuir 17 (2001) 1030, https://doi.org/10.1021/la001121f.

[49] D.A. Weitz, J.S. Huang, M.Y. Lin, J. Sung, Phys. Rev. Lett. 54 (1985) 1416, https://doi.org/10.1103/PhysRevLett.54.1416.

[50] S. Ikeda, E.A. Foegeding, T. Hagiwara, Langmuir 15 (1999) 8584, https://doi.org/10.1021/la9817415.

[51] D. Stauffer, A. Aharony, Introduction to percolation theory, Taylor & Francis, London, 1992.

[52] G. Hu, C. Zhao, S. Zhang, M. Yang, Z. Wang, Polymer 47 (2006) 480, https://doi.org/10.1016/j.polymer.2005.11.028.

[53] F.M. Blighe, Y.R. Hernandez, W.J. Blau, J.N. Coleman, Adv. Mater. 19 (2007) 4443, https://doi.org/10.1002/adma.200602912.

[54] Z. Fan, S.G. Advani, J. Rheol. 51 (2007) 585, https://doi.org/10.1122/1.2736424.

[55] M. Das, L. Chambon, Z. Varga, M. Vamvakaki, J.W. Swan, G. Petekidis, Soft Matter 17 (2021) 1232, https://doi.org/10.1039/D0SM01576H.

[56] C.O. Osuji, D.A. Weitz, Soft Matter 4 (2008) 1388, https://doi.org/10.1039/B716324J.

[57] X. Sha, K. Yu, H. Cao, K. Qian, J. Nanopart. Res. 15 (2013) 1816, https://doi.org/10.1007/s11051-013-1816-x.

[58] M. Hasanzadeh, V. Mottaghitalab, Rheol. Acta 55 (2016) 759, https://doi.org/10.1007/s00397-016-0950-7.

[59] C.O. Osuji, C. Kim, D.A. Weitz, Phys. Rev. E 77 (2008), 060402, https://doi.org/10.1103/PhysRevE.77.060402.

[60] F.J. Rubio-Hernández, J. Mol. Liq. 365 (2022) 120179, https://doi.org/10.1016/j.molliq.2022.120179.

[61] G. Żyła, J. Mol. Liq. 297 (2020), 111732, https://doi.org/10.1016/j.molliq.2019.111732.

[62] S. Lin-Gibson, J.A. Pathak, E.A. Grulke, H. Wang, E.K. Hobbie, Phys. Rev. Lett. 92 (2004), 048302, https://doi.org/10.1103/PhysRevLett.92.048302.

[63] Y. Wang, R.H. Ewoldt, J. Rheol. 66 (2022) 937, https://doi.org/10.1122/8.0000455.

[64] T. Divoux, V. Grenard, S. Manneville, Phys. Rev. Lett. 110 (2013), 018304, https://doi.org/10.1103/PhysRevLett.110.018304.

[65] J.B. Hipp, J.J. Richards, N.J. Wagner, J. Rheol. 63 (2019) 423, https://doi.org/10.1122/1.5071470.

[66] A. Narayanan, F. Mugele, M.H. Duits, Langmuir 33 (2017) 1629, https://doi.org/10.1021/acs.langmuir.6b04322.

[67] W.J. Tseng, S.-Y. Li, Mater. Sci. Eng., A 333 (2002) 314, https://doi.org/10.1016/S0921-5093(01)01856-1.

[68] K. Ke, Y. Wang, X.-Q. Liu, J. Cao, Y. Luo, W. Yang, B.-H. Xie, M.-B. Yang, Composites, Part B 43 (2012) 1425, https://doi.org/10.1016/j.compositesb.2011.09.007.

[69] B. Ploss, B. Ploss, F.G. Shin, H.L.W. Chan, C.L. Choy, Appl. Phys. Lett. 76 (2000) 2776, https://doi.org/10.1063/1.126472.

[70] M. Acosta, N. Novak, V. Rojas, S. Patel, R. Vaish, J. Koruza, G.A. Rossetti Jr., J. Rödel, Appl. Phys. Rev. 4 (2017), https://doi.org/10.1063/1.4990046.

[71] J. Briscoe, S. Dunn, Nano Energy 14 (2015) 15, https://doi.org/10.1016/j.nanoen.2014.11.059.